

α -decay calculations of heavy nuclei using an effective Skyrme interaction

D. E. Ward,* B. G. Carlsson, and S. Åberg

Division of Mathematical Physics, LTH, Lund University, P.O. Box 118, S-22100 Lund, Sweden

Background: For nuclei heavier than ^{208}Pb α decay is a dominating decay mode, and in the search of new superheavy elements one often observes chains of α decays.

Purpose: Explore and test microscopic descriptions of α decay based on theories with effective nuclear interactions.

Methods: The nuclear ground states are calculated with the Hartree-Fock-Bogoliubov (HFB) method using the Skyrme interaction. Microscopic α -decay formation amplitudes are calculated from the HFB wave functions, and the R -matrix formalism is utilized to obtain decay probabilities.

Results: Using a large harmonic-oscillator basis we obtain converged α -decay widths. A comparison with experiment including all spherical even-even α emitting nuclei shows that the model consistently predicts too small formation amplitudes while relative values are in good agreement with experiment.

Conclusions: The method was found to be numerically practical even with a large basis size. The comparison of formation amplitudes suggests that the pairing type correlations included in the HFB approach cannot produce sufficient α -particle clustering.

PACS numbers: 23.60.+e, 21.60.Jz, 21.10.Tg, 27.90.+b

I. INTRODUCTION

Superheavy elements (SHE) can be formed in heavy-ion fusion reactions, and typically α decay in several steps, see e.g. [1]. In a recent experiment [2] it has been possible to measure the emitted α particles in coincidence with γ radiation. This opens up possibilities to identify SHE through x rays, as well as to obtain detailed spectroscopic information. Such detailed nuclear structure experiments call for an accurate theoretical description that simultaneously provides a good prediction of both the structure of superheavy nuclei and the α -decay lifetimes. A good starting point is then to consider a microscopic model based on interacting nucleons where both the structure and the reaction parts can be treated on the same footing.

Calculations of α decay can be carried out at various levels of sophistication. Currently, most microscopic approaches are based on either microscopic-macroscopic models employing Woods-Saxon potentials combined with BCS pairing, or for some particular nuclei (e.g., ^{212}Po) using shell-model approaches where a few valence particles are allowed to interact via effective model-space interactions, see, e.g., Refs. [3, 4].

In this work, the structure model is based on modern and well-tested effective Skyrme interactions which allow for microscopic descriptions of nuclear properties throughout the nuclear chart. Wave functions of mother and daughter nuclei are obtained self-consistently using the Hartree-Fock-Bogoliubov (HFB) method and correlations are modeled using a density dependent zero-ranged pairing interaction. Taking the Skyrme interaction as a starting point allows different levels of correlations, that

are particularly important to describe the α -particle formation, to be subsequently included e.g. using the approach of [5].

A microscopic description of the α decay is obtained through the R -matrix approach [3, 4, 6] where the calculated wave functions of the mother and daughter nuclei are used to project out a formation amplitude for the α particle. Beyond the range of nuclear forces this amplitude is matched to the asymptotic Coulomb solution from which the flow of emitted α particles can be determined.

The method is quite general and can be applied to even-even as well as to odd nuclei [7]. Especially for odd nuclei it is important to have a reliable microscopic model to be able to predict the large variations in the half-lives for decays to different excited states. In this first study, we test the method for the description of α -decaying heavy, spherical even-even nuclei.

The paper is organized as follows. In Sec. II the theoretical formalism is described. We give the details of the nuclear structure model and review and discuss the treatment of α decay in the R -matrix approach. In Sec. III we investigate the convergence of the calculated formation amplitude, and its dependence on the parameters of the mean field and pairing force. Calculated α widths are compared to available experimental data on heavy near-spherical nuclei in Sec. IV, where the model also is applied to make predictions for α decay of the SHE near the predicted shell closures at $N = 184$, $Z = 114$ and 126. The results are discussed in Sec. V where in particular possible shortcomings and improvements of the model are considered. Finally, in Sec. VI we conclude and summarize the results.

* daniel.ward@matfys.lth.se

II. FORMALISM

In this section the formalism for our theoretical description of α decay is discussed. The ingredients of the nuclear structure model are provided in Sec. II A. An overview of the theoretical treatment of the α decay is given in Sec. II B, and in Sec. II C we describe how the formation amplitude is obtained.

A. Nuclear structure model

The ground states of the mother and daughter nuclei are described using the Hartree-Fock-Bogoliubov (HFB) method with an effective Skyrme interaction in the particle-hole channel [8]. The HFB equations are solved using an extended version of the program HOSPHE (v1.02) [9]. This code works with a spherical harmonic oscillator basis and can handle large basis sizes where the maximum oscillator shell included can be as high as $N_{\text{max}} = 70$. A large basis size is essential in order to obtain convergence for the α -particle formation amplitudes.

For the pairing a density-dependent zero-range δ interaction [10] combined with an energy truncation, $e_{\text{cut}}^{\text{e.s.}}$, in the equivalent spectra [11] is adopted. The pairing interaction is parametrized by

$$V_{\text{pair}}^q(\mathbf{r}, \mathbf{r}') = V_q \left[1 - \beta \frac{\rho(\mathbf{r})}{\rho_c} \right] \delta(\mathbf{r} - \mathbf{r}'), \quad q = n, p, \quad (1)$$

where $\rho_c = 0.16 \text{ fm}^{-3}$ is the saturation density of nuclear matter and β is a parameter determining the density dependence. In the case of so called surface pairing, i.e., $\beta = 1$, the pairing energy density gets its main contribution from the surface region. A density independent pairing is obtained when $\beta = 0$ in which case the main contribution comes from the nuclear interior. Pairing is treated both using the HFB approach and with an approximate version of the Lipkin-Nogami (LN) method [11]. The LN method provides an approximate particle-number restoration that gives more realistic pairing solutions and avoids the collapse of the pairing for magic nuclei obtained with the HFB method.

The proton pairing strength, V_p , is tuned so that the theoretical odd-even mass difference, $\Delta_p^{\text{th}}(N, Z)$, agrees with the experimental three-point gap centered on the odd nucleus,

$$\Delta_p^{\text{exp}}(N, Z) = E(N, Z+1) - \frac{1}{2}[E(N, Z) + E(N, Z+2)]. \quad (2)$$

To have a simple recipe we approximate $\Delta_p^{\text{th}}(N, Z)$ by the lowest quasiparticle energy E_p^{min} calculated for the even-even nucleus ${}_ZX_N$. The same prescription is used for the neutron pairing strength, V_n .

B. Decay treatment

α decay is treated microscopically using the same R -matrix-based approach that was used in Refs. [12–14] and reviewed in Ref. [3]. An important feature of α decay is the tunneling through the long-range Coulomb potential between the daughter nucleus and α particle. When the α particle is far away from the daughter nucleus with Z_D protons, their relative motion is described by an outgoing Coulomb wave function,

$$\frac{O_L(E, r)}{r} = \frac{1}{r} [G_L(\eta, \kappa r) + iF_L(\eta, \kappa r)], \quad (3)$$

where E is the resonance energy, L the angular momentum, F and G the regular and irregular Coulomb wave functions [15], $\kappa = \frac{\sqrt{2\mu E}}{\hbar}$ and $\eta = \frac{2Z_D\mu e^2}{\hbar^2\kappa}$, where μ is the reduced mass. In the R -matrix approach the system is divided into inner and outer regions. The solution for the relative motion in the inner region is matched to this outgoing Coulomb wave function at a matching radius, r_c . For the spherical case, the absolute width, Γ , of the α -decay with energy Q_α , is given by

$$\Gamma(r_c) = 2\gamma_0^2(r_c)P_0(Q_\alpha, r_c), \quad (4)$$

where γ_L is the reduced width,

$$\gamma_L^2(r_c) = \frac{\hbar^2}{2\mu r_c} r_c^2 g_L^2(r_c), \quad (5)$$

that depends on the formation amplitude, $g_L(r_c)$. The formation amplitude describes the relative α -daughter motion, and is obtained from the overlap of the mother nucleus with an α -particle and daughter nucleus separated by the distance r_c . P_L is the Coulomb penetrability factor,

$$P_L(Q_\alpha, r_c) = \frac{k_\alpha r_c}{|O_L(Q_\alpha, r_c)|^2}, \quad (6)$$

where $k_\alpha = \frac{\sqrt{2\mu Q_\alpha}}{\hbar}$. Both factors entering Eq. (4) depend on the matching radius, r_c . However, in an exact treatment these dependencies cancel and in the region where nuclear forces can be neglected Γ becomes constant. This constant value of the decay width is related to the half-life, $T_{1/2}$, through the usual formula $\Gamma = \hbar \ln 2 / T_{1/2}$.

The difference compared to earlier works is that we here obtain the wave functions for the mother and daughter nuclei entering in the formation amplitude using the Skyrme-HFB model employing a large harmonic-oscillator basis. To emphasize some of the approximations in the treatment, we will briefly discuss the main features of the so called BCS approach to α decay [3]. One can arrive to the formula (4) using either the Gamow state [16, 17], or the R -matrix formalism [6, 18]. A discussion on the difference between the two approaches,

when applied to proton decay, can be found in [19]. The main steps of the derivation are presented below from a similar perspective as in [20, 21].

We describe the mother nucleus, (M), as an exponentially decaying Gamow state [16]

$$\Psi_{IM}^{(M)}(\xi_D, \xi_\alpha, \mathbf{r}_{\alpha D}; t) = \Psi_{IM}^{(M)}(\xi_D, \xi_\alpha, \mathbf{r}_{\alpha D}; 0) e^{-i(E_M - i\frac{\Gamma}{2})t/\hbar}, \quad (7)$$

where I and M are the spin and spin projection of the mother nucleus, respectively. The Jacobi coordinate system $\xi_D, \xi_\alpha, \mathbf{r}_{\alpha D}$ corresponds to internal coordinates of the daughter nucleus and the α -particle, and a vector between their centers of mass. E_M and $-\Gamma/2$ are the real and imaginary parts of the complex energy of the Gamow state [22]. The state is normalized at $t = 0$ within some finite volume V :

$$\int_V \left| \Psi_{IM}^{(M)}(\xi_D, \xi_\alpha, \mathbf{r}_{\alpha D}; 0) \right|^2 d\xi_D d\xi_\alpha d\mathbf{r}_{\alpha D} = 1. \quad (8)$$

To find the rate of emitted α particles, one can start by approximating the mother nucleus as a combined state of daughter, (D), and valence particles, (v), from which the α particle is formed (see Appendix),

$$\Psi_{IM}^{(M)}(t=0) \simeq \mathcal{A}_{Dv} \left\{ \left[\Phi_J^{(D)}(\xi_D), \Phi_{L'}^{(v)}(\xi_\alpha, \mathbf{r}_{\alpha D}) \right]_{IM} \right\}, \quad (9)$$

where the operator \mathcal{A}_{Dv} [3] exchanges coordinates between the two parts in order to make the state fully antisymmetric.

For large distances between the α particle and the daughter nucleus, $r_{\alpha D}$, the components of the mother nucleus that contribute to the α -decay width are assumed to be described by the daughter nucleus wave function, $\Phi_{JM}^{(D)}(\xi_D)$, the spin zero intrinsic wave function of the α particle, $\Phi_{00}^{(\alpha)}(\xi_\alpha)$, and a wave function of their relative motion, $Y_{LM_L}(\hat{r}_{\alpha D})u_L(r_{\alpha D})$,

$$\mathcal{A}_{Dv} \left[\Phi_J^{(D)}(\xi_D), \Phi_0^{(\alpha)}(\xi_\alpha) Y_L(\hat{r}_{\alpha D}) u_L(r_{\alpha D}) \right]_{IM}. \quad (10)$$

The formation amplitude, $g_L(r_{\alpha D})$, is defined as the overlap between the mother nucleus wave function, $\Psi_{IM}^{(M)}$, and the intrinsic and angular parts of expression (10). With the approximation in Eq. (9), the formation amplitude can be expressed as

$$g_L(r_{\alpha D}) = \sum_{L'} \int \left[\Phi_J^{(D)}(\xi_D), \Phi_0^{(\alpha)}(\xi_\alpha) Y_L(\hat{r}_{\alpha D}) \right]_{IM}^* \times \left[\Phi_J^{(D)}(\xi_D), \Phi_{L'}^{(v)}(\xi_\alpha, \mathbf{r}_{\alpha D}) \right]_{IM} d\xi_D d\xi_\alpha d\hat{r}_{\alpha D}. \quad (11)$$

In this expression we have neglected the exchange between the α particle and the daughter nucleus. This is a valid approximation if the orbitals the α particle is expanded in are orthogonal to the orbitals of the daughter

nucleus. Clearly this is not fulfilled in general but is a good approximation when the α particle is sufficiently far away from the daughter nucleus. In this work we furthermore restrict ourselves to decay from ground states in spherical nuclei where mother and daughter nuclei both have spin zero, $J = 0$ and $I = 0$. This leads to the simpler form of the formation amplitude,

$$g_0(r_{\alpha D}) = \frac{1}{\sqrt{4\pi}} \int \Phi_{00}^{(\alpha)*}(\xi_\alpha) \Phi_{00}^{(v)}(\xi_\alpha, \mathbf{r}_{\alpha D}) d\xi_\alpha d\hat{r}_{\alpha D}. \quad (12)$$

The method of finding the wave functions entering this expression, further discussed below, involves an expansion in terms of harmonic oscillator basis functions. This implicitly imposes boundary conditions that the wave function goes to zero for large radii which is in principle incorrect. A Gamow state should instead have outgoing waves as boundary conditions. However, since the α particle has to penetrate a wide and high Coulomb barrier we can assume [3] that the harmonic oscillator basis can provide a good approximation inside the barrier, and use a matching condition to impose a tail with the correct asymptotic behavior.

For large distances, $r_{\alpha D}$, beyond the range of nuclear forces, the formation amplitude should behave as an outgoing Coulomb wave, see Eq. (3),

$$g_0^{\text{ext}}(Q_\alpha - i\Gamma/2, r_{\alpha D}) = C \frac{O_0(Q_\alpha - i\Gamma/2, r_{\alpha D})}{r_{\alpha D}}. \quad (13)$$

This expression is valid both inside and beyond the Coulomb barrier. The imaginary part of the energy causes the amplitude of O_0 to increase with $r_{\alpha D}$. Since Γ , related to the decay rate, is very small, this increase of the amplitude may be neglected inside the barrier. Neglecting the small Γ , the formation amplitude, Eq. (12), is matched to the external solution, Eq. (13), at the matching radius $r_{\alpha D} = r_c$, giving the total formation amplitude,

$$g_0^{\text{tot}}(r_{\alpha D}) = g_0(r_{\alpha D}) \theta(r_c - r_{\alpha D}) + g_0^{\text{ext}}(Q_\alpha, r_{\alpha D}) \theta(r_{\alpha D} - r_c), \quad (14)$$

where θ are Heaviside functions. The constant C in Eq. (13) is determined by requiring $g_0(r_c) = g_0^{\text{ext}}(r_c)$,

$$C = r_c \frac{g_0(r_c)}{O_0(Q_\alpha, r_c)}. \quad (15)$$

From the continuity equation, one can obtain the so-called current expression [17, 19]. It relates the width Γ to the probability flow, j_0 , at $t = 0$ through a surface at $r_{\alpha D} = r_0$. Choosing r_0 to correspond to the volume used for the normalization in Eq. (8) gives

$$\begin{aligned} \frac{\Gamma}{\hbar} &= \frac{i\hbar}{2\mu} r_0^2 \\ &\times \left[g_0^{\text{tot}}(r_0) \frac{\partial g_0^{\text{tot}*}(r_0)}{\partial r} - g_0^{\text{tot}*}(r_0) \frac{\partial g_0^{\text{tot}}(r_0)}{\partial r} \right] \\ &\equiv j_0(r_0), \end{aligned} \quad (16)$$

where we have assumed that α decay is the only decay channel contributing to the probability flow. Since we neglect the complex part of the energy the flow through two different spheres that both enclose the origin is equal, and one may for simplicity evaluate the flow $j_0(r)$ in the $r \rightarrow \infty$ limit. Inserting the asymptotic form of $O_0(Q_\alpha, r)$ for large r [15] in Eq. (16) gives

$$j_0(r_0) = \lim_{r \rightarrow \infty} j_0(r) = |C|^2 \frac{\hbar k_\alpha}{\mu}. \quad (17)$$

Combining Eqs. (15), (16) and (17) we recover formula (4),

$$\Gamma = \frac{r_c^2 g_0^2(r_c) \hbar^2 k_\alpha}{|O_0(Q_\alpha, r_c)|^2 \mu} = 2\gamma_0^2(r_c) P_0(Q_\alpha, r_c). \quad (18)$$

C. Formation amplitude

We use the standard coordinate system, $(\mathbf{R}_\alpha, \xi_\alpha)$, with $\xi_\alpha = (\mathbf{r}_\pi, \mathbf{r}_\nu, \mathbf{r}_\alpha)$, where [4]:

$$\begin{aligned} \mathbf{r}_\pi &= \frac{\mathbf{r}_1 - \mathbf{r}_2}{\sqrt{2}}, \quad \mathbf{r}_\nu = \frac{\mathbf{r}_3 - \mathbf{r}_4}{\sqrt{2}}, \\ \mathbf{r}_\alpha &= \frac{1}{2}(\mathbf{r}_1 + \mathbf{r}_2 - \mathbf{r}_3 - \mathbf{r}_4), \end{aligned}$$

and

$$\mathbf{R}_\alpha = \frac{1}{2}(\mathbf{r}_1 + \mathbf{r}_2 + \mathbf{r}_3 + \mathbf{r}_4). \quad (19)$$

Here $\mathbf{r}_1, \mathbf{r}_2$ are the coordinates for the valence protons, and $\mathbf{r}_3, \mathbf{r}_4$ for the valence neutrons. The Jacobian for the transformation $(\mathbf{r}_1, \mathbf{r}_2, \mathbf{r}_3, \mathbf{r}_4) \rightarrow (\mathbf{R}_\alpha, \mathbf{r}_\alpha, \mathbf{r}_\pi, \mathbf{r}_\nu)$ is 1.

To preserve translational invariance, the valence wave function $\Phi_{00}^{(v)}(\xi_\alpha, \mathbf{r}_{\alpha D})$ entering in Eq. (12) should describe the motion of the valence particles relative to the daughter. From the nuclear structure model we obtain shell model type wave functions, which are localized in a laboratory coordinate system, and we approximate the formation amplitude, (12), by

$$g_0(R) = \frac{1}{\sqrt{4\pi}} \int \Phi_0^{(\alpha)*}(\xi_\alpha) \sqrt{8} \tilde{\Phi}_{00}^{(v)}(\xi_\alpha, 2\mathbf{R}) d\xi_\alpha d\hat{R}, \quad (20)$$

where $\mathbf{R} = \mathbf{R}_\alpha/2$ is the center-of-mass coordinate of the α particle, and $\tilde{\Phi}_{00}^{(v)}(\xi_\alpha, \mathbf{R}_\alpha)$ is the valence nucleon wave function of the localized mother nucleus, discussed in the Appendix. The approximation in Eq. (20) consists of making the substitution $\mathbf{r}_{\alpha D} \rightarrow \mathbf{R}$ and using a localized valence nucleon wave function. This approximation is justified when the daughter nucleus is heavy relative to the α particle, and the center of mass parts of the laboratory system wave functions for mother and daughter nuclei are well localized [23]. The factor of $\sqrt{8}$ arises to preserve the normalization of the valence nucleon wave function, when expressed in the coordinate \mathbf{R} [24], as can be seen from

$$|\tilde{\Phi}_{00}^{(v)}(\xi_\alpha, \mathbf{R}_\alpha)|^2 d^3 R_\alpha = |\tilde{\Phi}_{00}^{(v)}(\xi_\alpha, \mathbf{R}_\alpha(\mathbf{R}))|^2 8 d^3 R. \quad (21)$$

For the intrinsic α -particle wave function $\Phi_{00}^{(\alpha)}(\xi_\alpha)$, we use the standard approximation [4],

$$\begin{aligned} \Phi_{00}^{(\alpha)}(\mathbf{r}_\pi, \mathbf{r}_\nu, \mathbf{r}_\alpha, s_1, s_2, s_3, s_4) \\ = \left(\frac{1}{b_\alpha^3 \pi^{3/2}} \right)^{3/2} e^{-\frac{r_\pi^2 + r_\nu^2 + r_\alpha^2}{2b_\alpha^2}} \\ \times [\chi_{\frac{1}{2}}(s_1), \chi_{\frac{1}{2}}(s_2)]_{00} [\chi_{\frac{1}{2}}(s_3), \chi_{\frac{1}{2}}(s_4)]_{00}, \end{aligned} \quad (22)$$

where $\chi_{\frac{1}{2}}(s)$ are spin wave functions. In order to agree with electron scattering experiments the oscillator length b_α should be chosen as $b_\alpha \simeq \sqrt{2}$ fm [4] and we adopt the value $b_\alpha = 1.42$ fm throughout.

Inserting the approximate valence nucleon wave function, Eq. (A.10), transformed to relative and total coordinates [25], and the α -particle wave function, Eq. (22) into Eq. (20) gives the final expression for the formation amplitude

$$\begin{aligned} g_0(R) &= \frac{1}{\sqrt{2}} \sum_{l_\pi j_\pi} \sum_{n_\pi n'_\pi} \frac{X_{n_\pi n'_\pi}^{l_\pi j_\pi} \hat{j}_\pi^2}{\hat{l}_\pi} \sum_{l_\nu j_\nu} \sum_{n_\nu n'_\nu} \frac{X_{n_\nu n'_\nu}^{l_\nu j_\nu} \hat{j}_\nu^2}{\hat{l}_\nu} \\ &\times \sum_{N_{12} n_{12}} \langle N_{12} 0, n_{12} 0; 0 | n_\pi l_\pi, n'_\pi l_\pi; 0 \rangle \\ &\times \sum_{N_{34} n_{34}} \langle N_{34} 0, n_{34} 0; 0 | n_\nu l_\nu, n'_\nu l_\nu; 0 \rangle \\ &\times \sum_{N_\alpha n_\alpha} \langle N_\alpha 0, n_\alpha 0; 0 | N_{12} 0, N_{34} 0; 0 \rangle \\ &\times I_{n_\alpha}^{(b, b_\alpha)} I_{n_{12}}^{(b, b_\alpha)} I_{n_{34}}^{(b, b_\alpha)} R_{N_\alpha 0}^{(b)}(2R), \end{aligned} \quad (23)$$

where $\hat{j} = \sqrt{j(j+1)}$ and

$$I_n^{(b, b_\alpha)} = \int r^2 dr R_{00}^{(b_\alpha)*}(r) R_{n0}^{(b)}(r). \quad (24)$$

$R_{nl}^{(b)}(r)$ is here the radial part of a spherical oscillator wave function with n nodes and angular momentum l , and b denotes the oscillator length used for the basis.

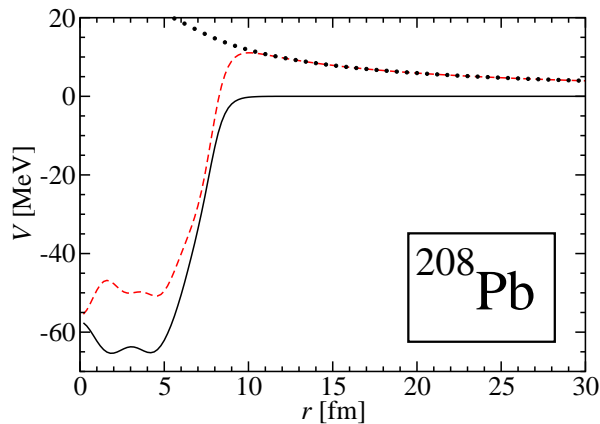


Figure 1. (Color online) Local mean fields [26] for ^{208}Pb , from the SLy4 Skyrme force. The solid line shows the field for neutrons, the dashed line for protons, and the dotted line shows the Coulomb part of the proton mean-field.

III. DEPENDENCE ON MEAN FIELD AND PAIRING FORCE

In this section we investigate the dependence of the formation amplitude on the mean field and pairing force. In Sec. III A we check that the dimension of the oscillator basis is sufficient to obtain correct density at large radii, and that the α -particle formation amplitude converges. The sensitivity of the formation amplitude to the type of Skyrme force used is studied in Sec. III B, the role of approximate particle number correction in the HFB solution is considered in Sec. III C, and the role of surface or volume pairing in Sec. III D.

A. Convergence of the formation amplitude

To have confidence in the numerical results, one must make sure that the obtained formation amplitude does not depend on the size of the oscillator basis. The formation amplitude must also be converged for large separations of α particle and daughter nucleus, so that nuclear forces between the clusters can be neglected.

This implies several criteria that should be fulfilled for the numerical calculation, the most obvious being a sufficient accuracy for the tails of the nuclear wave functions. To satisfy the condition of vanishing nuclear forces between the clusters, the tails should be accurately calculated to a distance at least as large as the distance where the nuclear mean field acting on the valence nucleons becomes negligible.

At the HFB level of approximation the nuclear interactions give rise to density dependent fields. The local mean fields $V(r)$ [26] for protons and neutrons of double magic lead are shown in Fig. 1. They were obtained from a converged solution of the HFB equations using the code HFBRAD [27] with the SLy4 Skyrme interaction. The densities from this code are obtained by solving the HFB-

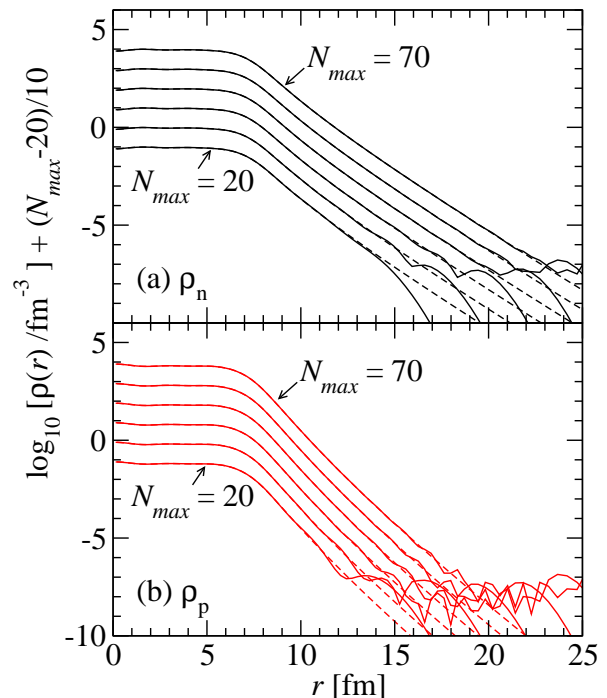


Figure 2. (Color online) The upper(lower) panel shows neutron(proton) densities for ^{208}Pb obtained by solving the HFB equations using a spherical oscillator basis (solid lines) and solving on a radial grid (dashed lines). To separate the different lines, the densities are multiplied by a factor $10^{(N_{\text{max}}/10-2)}$.

equations in r -space in a large box, that give converged results out to very large radii. It is seen that for $r \geq 10$ fm the neutron and proton nuclear fields are close to zero, and only the Coulomb potential contributes. Thus the condition of vanishing nuclear forces should be approximately satisfied at α -daughter separations larger than 10 fm.

To investigate what size of the spherical oscillator basis is needed for such wave functions, the neutron and proton densities from using different number of major oscillator shells are shown in Fig. 2, where also the results from HFBAD are shown. Including oscillator shells up to $N_{\text{max}} = 20$ gives converged densities out to around 10 fm. It is seen how each increase of the oscillator size by ten units ($N_{\text{max}} = 30, 40, \dots$) increases the convergence radius by an additional 1–2 fm. Similar trends are found for the pairing density. We find that HFB calculations for ^{212}Po give converged pairing density at $r = 10$ fm when $N_{\text{max}} \geq 20$.

The effect of the cutoff in the pairing calculation was tested using cut-off energies $e_{\text{cut}}^{\text{e.s.}} = 30, 60$ and 90 MeV. When the pairing strength is tuned so that $\Delta_{\text{exp}}(N = 128, Z = 84)$, Eq. (2), is reproduced, the effect on the formation amplitudes from the different cutoffs was small, and we shall use $e_{\text{cut}}^{\text{e.s.}} = 60$ MeV throughout.

To investigate convergence, the R -matrix decay width $\Gamma(r)$ is calculated for ^{212}Po . The mother and daugh-

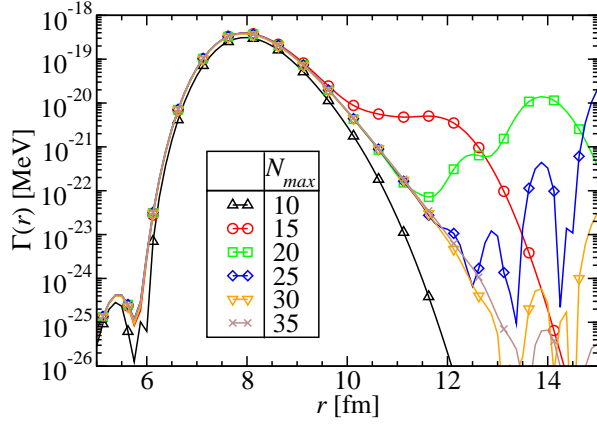


Figure 3. (Color online) Decay width Γ for ^{212}Po calculated for different sizes of the oscillator basis.

ter wave functions are obtained from the SLy4 HFB+LN prescription, and the experimental Q_α value [28] is used in the decay width expression, Eq. (4). As can be seen in Fig. 3 the results converge to larger distances as the basis size is gradually increased from $N_{\text{max}} = 10$ to $N_{\text{max}} = 35$. For $N_{\text{max}} = 15$ the results are converged to around 9 fm, while for the largest basis to around 13 fm. By using a basis with $N_{\text{max}} \geq 25$ a converged formation amplitude is obtained for separations beyond the range of inter-cluster nuclear forces. To avoid numerical errors $N_{\text{max}} = 30$ will be used throughout.

B. Skyrme force parameters

Several fits of Skyrme force parameters exist that give reasonable results for ground-state observables such as binding energy and rms-radii [8]. The impact on the microscopic decay width from the use of different Skyrme forces was tested employing volume pairing with the LN method. For each Skyrme force the pairing strength was refitted. The decay width for ^{212}Po using SLy4, SKM* and SKX interactions are shown in Fig. 4. The results show a negligible difference between SLy4 and SKM*, while for SKX the decay width is a factor 3.7 smaller at $r = 9$ fm. In general, the results are quite insensitive to the details of the effective particle-hole interaction, and the SLy4 effective interaction will be used throughout this paper.

C. Particle number correction

Approximate particle number projection with the LN procedure allows pairing solutions also when there is a large gap around the Fermi level in the single-particle spectrum. As discussed below, pairing correlations have a dramatic effect on the decay widths [3]. Avoiding a collapse of the pairing for magic and semimagic nuclei the formation amplitude increases considerably. This is

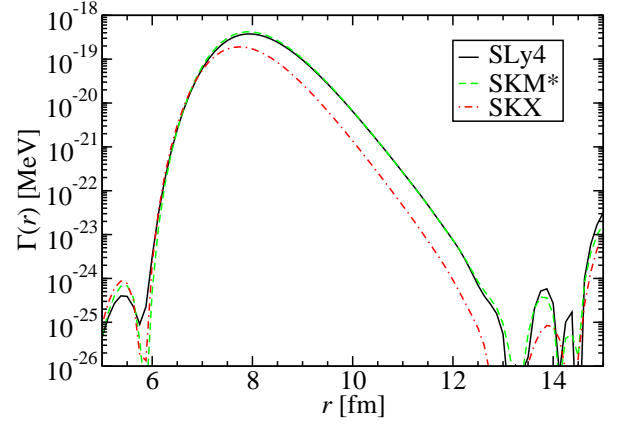


Figure 4. (Color online) Decay width Γ for ^{212}Po . Calculated using three different Skyrme forces.

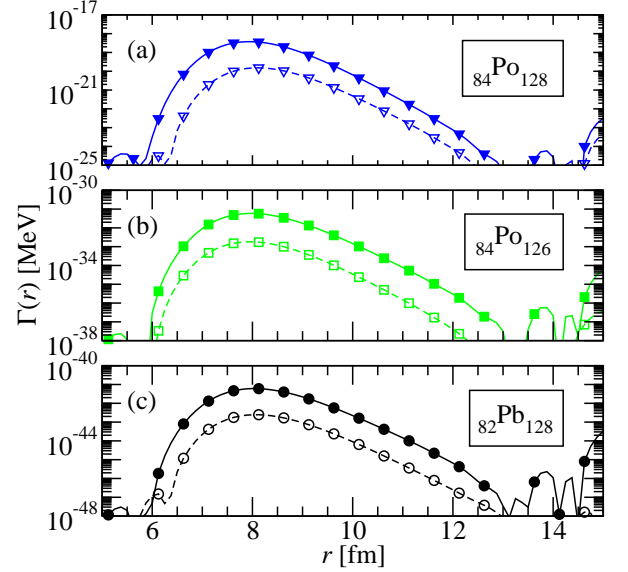


Figure 5. (Color online) Effect on decay rate of approximate particle number restoration with the Lipkin-Nogami procedure. The three panels show results for ^{212}Po , ^{210}Po , and ^{210}Pb , respectively. The decay width using HFB+LN wave functions are shown with full lines and solid symbols. Dashed lines with outlined symbols show results when standard HFB calculations were performed.

illustrated in Fig. 5, where decay widths obtained with and without the approximate particle number projection are compared. The increase at $r = 9.0$ fm for the g.s. to g.s. α decay of $^{212}_{84}\text{Po}_{128}$, $^{210}_{84}\text{Po}_{126}$ and $^{210}_{82}\text{Pb}_{128}$, is a factor 17, 36, and 24, respectively. Two factors influencing the microscopic decay width are the amount of overlap of the least bound, or valence, nucleons of the mother nucleus with an α particle, and the overlap of the remaining nucleons with the daughter. A possible explanation why the largest enhancement factors are obtained for the semimagic ^{210}Po and ^{210}Pb nuclei is that in these cases the avoided pairing collapse causes an increase of both

types of overlaps compared to just one type of overlap in the case of ^{212}Po .

D. Density dependence of pairing force - ^{212}Po example

Since ^{212}Po has a simple structure with two protons and two neutrons outside a core of doubly magic lead it is often used to test microscopic α -decay theories. The experimental decay width for the g.s. to g.s. α decay of this nucleus is $\Gamma_{\text{exp}} = 1.53 \times 10^{-15}$ MeV [28]. The converged R -matrix decay width shown in Fig. 3 is a factor 2.4×10^{-4} smaller than the experimental value at the stationary point around $r = 8$ fm. The down-sloping function $\Gamma(r)$ for larger r also shows that inside the Coulomb barrier the calculated formation amplitude has a slope corresponding to an α particle that is considerably more bound to the daughter than observed experimentally.

Including a density dependence in the effective pairing interaction allows for a description where the pairing correlations in the surface of the nucleus is increased, and the correlations in the nuclear interior is decreased. To see to what extent an increased pairing in the surface region might favor the formation of α particles, the decay width of ^{212}Po was calculated assuming different density dependencies of the pairing. To get consistent results the pairing strengths are refitted in each case.

The density dependence is determined by the parameter β in Eq. (1), where $\beta = 0$ gives volume pairing and $\beta = 1$ amounts to surface pairing. The decay widths obtained from these two choices are shown in Fig. 6. One notices that the width increases by almost one order of magnitude when surface pairing is used instead of volume pairing. The negative slope of the decay width is also reduced, indicating that the slope of the formation amplitude follows the slope of the outgoing Coulomb wave function slightly better. This corresponds to a formed α particle that is slightly less bound to the daughter nucleus, as compared to when volume pairing is used. The effect is however not sufficient to give an α -particle amplitude reproducing experimental data.

Additional clustering in the surface can be introduced by formally setting $\beta > 1$. This corresponds to a force which is repulsive in the nuclear interior, and strongly attractive in the surface. It is included as an extreme case; in fact, fits of ground-state properties suggest that the density dependence of the effective pairing force should be $0 \leq \beta \leq 0.5$ [29]. Figure 6 shows that setting $\beta = 1.3$ gives an additional increase of the decay width, as compared to the case of $\beta = 1$, although it is still well below the experimental value.

To test the limits of the pairing force in providing α clustering, we also show in Fig. 6 (dashed lines) results of a calculation where the pairing strengths are increased to produce a gap twice as large as the experimental pairing gap, $\Delta_{\text{th}} = 2\Delta_{\text{exp}}$. It is seen that even in this extreme case the pairing force is unable to provide a sufficiently

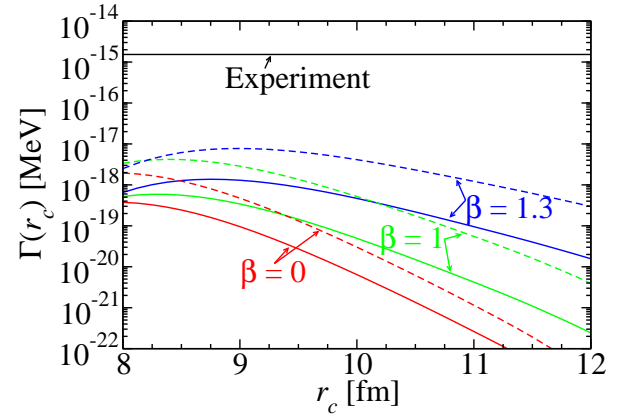


Figure 6. (Color online) Decay width for ^{212}Po . The effective interaction SLY4 was used together with zero range pairing with different density dependence: volume $\beta = 0$, surface $\beta = 1.0$, anti-volume $\beta = 1.3$. The dashed lines show results for large pairing fit to twice the experimental odd-even gaps. The straight line shows the experimental value.

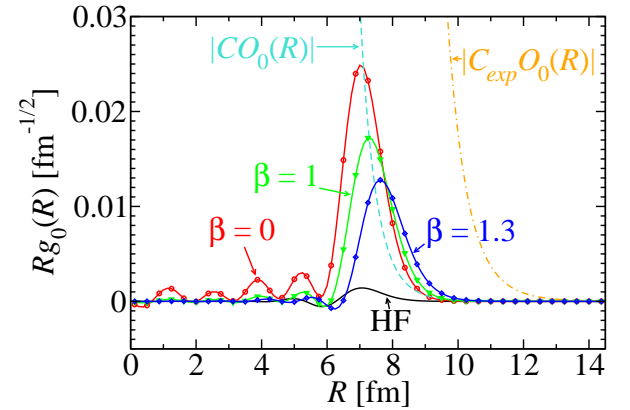


Figure 7. (Color online) Formation amplitude $Rg_0(R)$ for ^{212}Po obtained using different pairing prescriptions. Solid lines show results from microscopic calculations. Outgoing Coulomb wave functions are shown by dashed and dot-dashed lines, see text for details.

large decay width.

Figure 7 shows the formation amplitudes, $Rg_0(R)$, Eq. (20), for $\beta = 0, 1$, and 1.3 . Also shown are results from calculations with negligible pairing, equivalent to solving the Hartree-Fock equations, denoted by HF. As can be seen in the figure, the correlations induced by the pairing greatly increase the formation amplitude compared to the HF results. At $r = 9.0$ fm for the case $\beta = 0$ the increase is a factor 16.8, corresponding to a factor 281 larger decay width.

The modulus of the outgoing Coulomb wave function for the external region, $Rg_0^{\text{ext}}(Q_\alpha^{\text{exp}}, R) = CO_0(R)$, Eq. (13), fitted to the $\beta = 0$ formation amplitude at the matching radius $r_c = 9$ fm is shown by the dashed line. This outgoing Coulomb wave function is not a valid solution in the interior of the nucleus, and increases rapidly

with decreasing radius. Examining the tails of the formation amplitude and the Coulomb wave function, which are too small to be visible in Fig. 7, we note that the formation amplitude decreases more rapidly as a function of R , which is the reason why we do not obtain a flat plateau for $\Gamma(r_c)$ in Fig. 6.

Using Eq. (18) we can find the external wave function which would perfectly reproduce experiment. This gives $Rg_{\text{exp}}^{\text{ext}}(Q_{\alpha}^{\text{exp}}, R) = C_{\text{exp}} O_0(R)$, with $|C_{\text{exp}}| = \sqrt{\frac{\Gamma_{\text{exp}}}{h}} \sqrt{\frac{\mu}{2Q_{\alpha}^{\text{exp}}}}$, and is shown by the dot-dashed line in Fig. 7. Comparing the two external wave functions, one notes that to obtain a plateau for $\Gamma(r_t)$ with value Γ_{exp} the microscopic formation amplitudes should be pushed out further beyond the nuclear surface, and the slope of the tails should be slightly reduced.

IV. REDUCED WIDTHS COMPARED WITH EXPERIMENT

Even though the model does not produce the right slope and magnitude of the tail, the formation amplitude depends on the amount of structural overlap of the mother nucleus with the α -daughter configuration. To be able to reasonably calculate the decay width, some approximate prescription must be adopted. From the discussion above we see that the formation amplitude in the nuclear surface must be increased. Assuming that for all nuclei the correct formation amplitude in the surface is proportional to the calculated microscopic formation amplitude, a constant renormalization factor is obtained. Calculated structural variations in the formation amplitude will then be preserved and the calculated α -decay widths may be compared to experimental data. Below we perform such an effective description of α -decay widths of all heavy, even-even near-spherical nuclei with measured decay widths. We also apply the method to predict decay widths for some α -decaying superheavy elements.

The decay widths are calculated using experimental Q_{α} values from [28]. The formation amplitudes are matched to outgoing Coulomb wave functions in the nuclear surface at the touching radius r_t defined by [12]

$$r_t = r_0 \left[(A - 4)^{1/3} + 4^{1/3} \right], \quad (25)$$

with $r_0 = 1.2$ fm. The touching radius gives an approximate radius beyond which the α particle and daughter nucleus matter densities would be separated, which for ^{212}Po is $r_t = 9.01$ fm. At this radius the attractive forces between α and daughter are not completely negligible (cf. Fig. 1), but we find that the normalized decay widths depend weakly on r_0 .

For the nuclear structure calculation the SLy4 [30] Skyrme effective nucleon-nucleon potential is used in the particle-hole channel. The pairing is treated using the Lipkin-Nogami prescription. Both volume, $\beta = 0$, and

Table I. Pairing strengths used in this work.

	β	$V_n [\text{MeVfm}^3]$	$V_p [\text{MeVfm}^3]$
SLy4	0	-190.5	-180.5
SLy4+LN	0	-182	-175
SLy4+LN	1.0	-443	-530
SLy4+LN	1.3	-555	-770

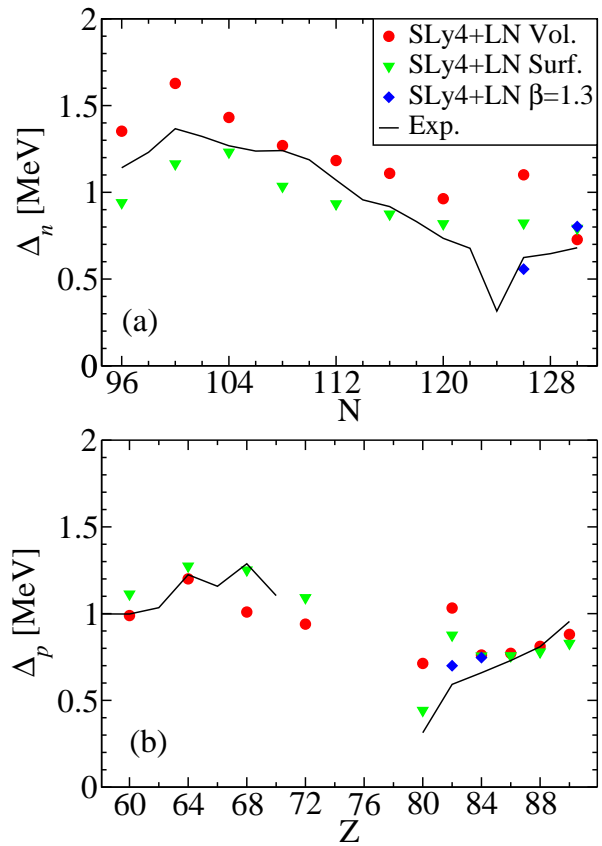


Figure 8. (Color online) Upper(lower) panel: neutron(proton) pairing gaps for proton(neutron)-magic nuclei with neutron(proton) number, $N(Z)$. The theoretical and experimental pairing gaps, $\Delta_{n(p)}$, are obtained as described in Sec. II A.

surface, $\beta = 1$, pairing types are used [Eq. (1)]. The pairing strengths used are shown in Table I. Calculated odd-even gaps for several semimagic nuclei are compared to experiment in Fig. 8. The experimental variation of the pair gap with particle number is found to be fairly well reproduced by both pairing recipes $\beta = 0$ and $\beta = 1$.

Using this prescription the ground state to ground state α -decay widths are determined for all even-even α emitters included in the compilation of experimental data in [28], and where the theoretical mass table of Möller and Nix [31] predicts a near-spherical ground state with quadrupole deformation parameter $|\beta_2| \leq 0.1$ for both mother and daughter nuclei. This amounts in total to 48 different α emitters.

The theoretical decay widths, $\Gamma_{\text{th}} = \Gamma(r_t)$, divided by

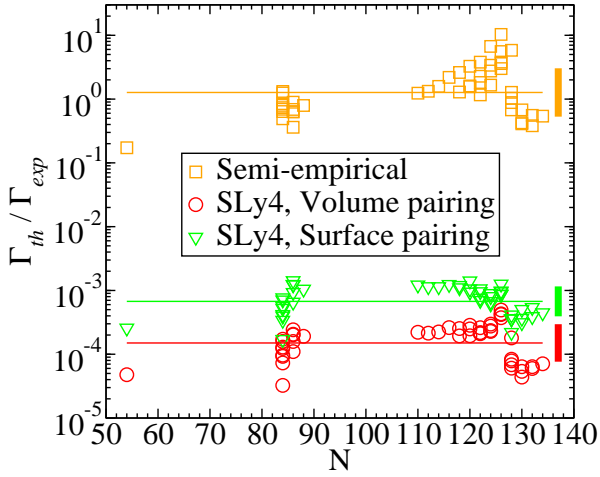


Figure 9. (Color online) Theoretical decay widths obtained from the UDL (squares), SLy4 with volume pairing (circles), and surface pairing (triangles) divided by the experimental value are shown versus the neutron number of the decaying nucleus. For each model calculation horizontal lines and vertical bars denote mean and standard deviation, respectively.

the experimental widths, Γ_{exp} , are shown in Fig. 9. For the surface pairing type calculations all 48 near-spherical even-even α emitters are included, while ^{218}U is missing from the volume pairing type calculation due to numerical convergence problems. For comparison predictions from a semi-empirical model are also shown. This model, *Universal Decay Law* (UDL) [32], is based on the R -matrix expression (4) but the formation amplitude is parametrized with three free parameters fitted to data. Here we consider parameter set I, which is fitted to even-even α -decay data. As seen in Fig. 9, for the UDL the results for the ratio $\Gamma_{\text{th}}/\Gamma_{\text{exp}}$ vary around a mean value close to 1. The microscopic models systematically produce too small decay widths, with slightly better agreement for the surface pairing. The variation around the mean trend is smaller for the microscopic models than the results from the UDL, especially around the $N = 126$ shell closure.

The logarithmic mean deviation, \mathcal{M} , from experimental data,

$$\mathcal{M} = \frac{1}{n} \sum_{i=1}^n \log_{10}[\Gamma_{\text{th}}^{(i)}/\Gamma_{\text{exp}}^{(i)}], \quad (26)$$

and corresponding standard deviation σ , are given in Table II for each of the calculations. The theoretical results using volume or surface pairing underestimates the decay width by 3 to 4 orders of magnitude, but follow structural changes in the experimental data quite well. This can be seen by fairly small σ values, that are indeed smaller than those obtained with the UDL.

The renormalized decay width is now introduced as

$$\tilde{\Gamma}_{\text{th}}^{(i)} = 10^{-\mathcal{M}} \Gamma_{\text{th}}^{(i)}, \quad (27)$$

Table II. Mean, \mathcal{M} , and standard deviation, σ , of $\log_{10}[\Gamma_{\text{th}}/\Gamma_{\text{exp}}]$ for all included nuclei for the three different models in Fig. 9:

	\mathcal{M}	σ
SLy4, Volume pairing	-3.82	0.29
SLy4, Surface pairing	-3.17	0.23
UDL	0.10	0.38

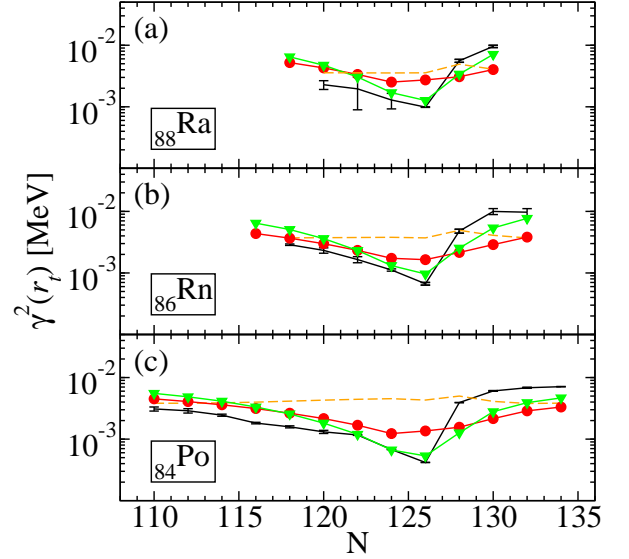


Figure 10. (Color online) Reduced width at the touching radius for three isotope chains as a function of neutron number. The error-bars show extracted experimental reduced widths. Circles and triangles show the renormalized $\tilde{\gamma}^2$, Eq. (28), obtained from volume and surface pairing, respectively. The dashed line shows results from the UDL.

and correspondingly for the reduced width

$$\tilde{\gamma}^2(r_t) = 10^{-\mathcal{M}} \gamma^2(r_t). \quad (28)$$

In Fig. 10 calculated renormalized reduced widths are compared to experimental data for isotope chains of Po ($Z = 84$), Rn ($Z = 86$) and Ra ($Z = 88$) nuclei.

The experimental reduced widths show a smoothly decreasing trend as a function of neutron number towards the shell closure at 126. When crossing the shell gap, the experimental value increases by about an order of magnitude, after which there is a smoothly increasing trend. Comparing volume and surface pairing the smooth behavior in the open-shell regions is captured fairly well by both pairing models. However, surface pairing consistently captures the magnitude of the jump when crossing $N = 126$, as well as the trends in the data, better than the volume type pairing. While the UDL reproduces the correct mean value, it does not follow the fluctuations around the shell closure.

Figure 11 shows the same quantities but for α emitters with neutron numbers 84 and 86. The main deviation from the experimental trend is that, for the $N = 84$

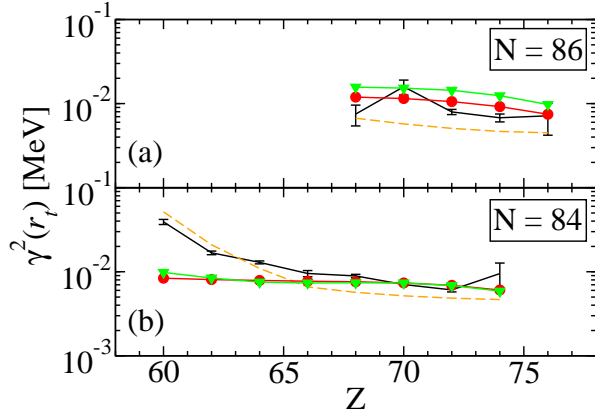


Figure 11. (Color online) Similar to Fig. 10 but for the isobar chains $N = 84$, and $N = 86$ as a function of proton number.

Table III. T denotes half-lives from renormalized microscopic calculations with $\beta = 1$. Predictions from the semi-empirical formula are given by T_{UDL} .

Nucleus	Q_{α}^{th} [MeV]	T [s]	T_{UDL} [s]
$^{294}_{114}180$	9.11	593	264
$^{296}_{114}182$	9.13	523	210
$^{298}_{114}184$	9.09	571	264
$^{300}_{114}186$	10.07	0.376	0.248
$^{306}_{126}180$	16.23	2.20×10^{-9}	1.20×10^{-10}
$^{308}_{126}182$	16.25	2.25×10^{-9}	1.03×10^{-10}
$^{310}_{126}184$	16.25	2.61×10^{-9}	9.52×10^{-11}
$^{312}_{126}186$	16.64	4.77×10^{-10}	2.29×10^{-11}

isotones, the microscopic results fail to capture the increased formation amplitude with decreasing Z . Here the best agreement with data is obtained from the UDL, suggesting small structural changes for the $N = 84$ isotones.

We apply the same prescription to make predictions for the α decay of the predicted near-spherical superheavy elements with $Z = 114, 126$ and $N = 180, 182, 184, 186$. The microscopic results are obtained using surface pairing, $\beta = 1$, and renormalized using Eqs. (27) and (28). The theoretical Q_{α} values of Refs. [33, 34] are used. The predicted half-lives are shown in Table III. The corresponding reduced width amplitudes are shown in Fig. 12. For the $Z = 114$ isotopes, the difference between the microscopic and semi-empirical reduced width is less than a factor 3, i.e., the microscopic model does not predict any dramatic structural effect that might lead to especially long lifetimes for these superheavy isotopes. The microscopic reduced widths increase by roughly a factor 2 when crossing the $N = 184$ gap, similar to the situation for $N = 126$, shown in Fig. 10. The much shorter predicted half-life for $^{300}_{114}186$ compared to $^{294-298}_{114}180-184$ is due to the ~ 1 MeV larger predicted Q_{α} value for this nucleus, see Table III. Thus, for predictions of life-times, uncertainty in the predicted Q_{α} values has a much larger effect than the difference in the reduced widths obtained

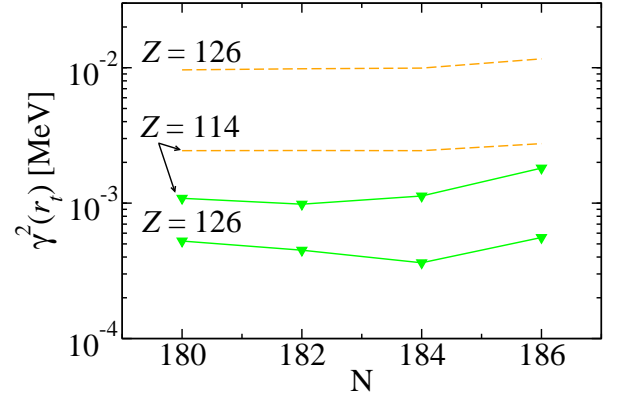


Figure 12. (Color online) Reduced widths at the touching radius for the SHE of Table III. The triangles show the renormalized microscopic results, from $\beta = 1$. The dashed lines show results obtained using the UDL.

from the semi-empirical and microscopic models.

Extrapolating further to the region around $^{310}_{126}184$, the results from the two models start to differ more. The $N = 184$ shell gap implies a cusp in the microscopically calculated reduced widths, while a smooth behavior is seen for the semi-empirical UDL. On the average, the reduced widths from the microscopic model are roughly a factor 20 smaller than the corresponding values from the UDL. This gives the order of magnitude longer half-lives obtained from the microscopic calculation.

V. DISCUSSION

The calculated decay widths show that the decay rates are systematically underestimated when the HFB formation amplitudes are used. As with any process depending on tunneling through a Coulomb barrier, the asymptotics and thus the flow of particles are extremely sensitive to the decay energy. For heavy nuclei it is a difficult task to predict observables such as one-particle separation energies and resonances with sufficient accuracy for spectroscopy. One can then assume that for a more complicated process such as α -particle formation, the energy dependent tail of the formation amplitude will never be described with accuracy comparable to the uncertainties in the experimental measurement of decay energies, and that this problem will exist to some degree for even the most sophisticated model. To obtain quantitative agreement with data, some type of renormalization must be employed.

Here we have adopted the simple procedure consisting of using the experimental Q_{α} value for the outgoing Coulomb wave function, combined with renormalizing the decay width by multiplying with one free parameter. The procedure includes a choice of matching radius, here chosen as the touching radius, as any mismatch in the slope of the microscopic formation amplitude compared to the Coulomb wave function produces an r_c dependence

of the R -matrix decay width.

Examples of other approaches to renormalize the formation amplitude can be found in the literature: In Ref. [35], the properties of the single-particle basis were tuned as an effective prescription to reproduce the correct absolute value and slope of the formation amplitude. In Ref. [36], in addition to the R -matrix expression for $\Gamma(r_c)$, Eq. (4), a reaction theoretical prescription was used. In this prescription the formation amplitude, corrected for anti-symmetrization in the nuclear interior, was integrated giving a spectroscopic factor. The decay was then treated on the one-body level using a local optical model α -daughter potential which can be adjusted to produce the correct resonance energy.

In order to get an idea what could be improved in the present α -decay approach we list five additional effects that could be taken into account and try to estimate their influence:

1. *Antisymmetrization*: The exchange between the α particle and the daughter nucleus can only be neglected for large separations r . It is possible to modify the formation amplitude to take exchange effects into account [37, 38]. For small r this results in a large increase of the formation amplitude, while for large r the modified formation amplitude reduces to the $g(r)$ used here. The value of r where $g(r)$ starts to be a good approximation depends on the daughter and α -particle wave functions and thus varies from case to case. Both types of formation amplitudes were calculated for ^{212}Po in [23, 36]. In [23] the correction amounted to an increase by a factor ≈ 2 , and in [36] a factor ≈ 3 for the formation amplitude at $r = 9$ fm. Such a correction amounts to an increase by a factor of 4 or 9 respectively in the decay width.
2. *Center-of-mass (c.m.) corrections*: In this article and in most previous studies the formation amplitudes are evaluated with shell-model wave functions instead of intrinsic states where the c.m. motion is separated out. The effect of correcting for the c.m. motion was studied in Ref. [23]. It is clear from the formulas presented in this reference that the correction is most important for light nuclei and will increase the absolute values of the formation amplitudes as well as stretching the formation amplitudes, it will thus move their maxima to larger radii in better agreement with experiment.
3. *Exact Coulomb exchange*: In this work we take the direct part of the Coulomb interaction into account and treat the exchange part in a Slater approximation [40]. The asymptotic dependence of the Coulomb potential for a proton should be $v(r) = \frac{e^2(Z-1)}{r}$ but becomes $v(r) = \frac{e^2 Z}{r}$ with the Slater approximation. Using exact Coulomb exchange will thus change the slope of the potential felt by the α particle and make it less bound in

the calculations as well as increasing its magnitude somewhat. However, for a heavy system such as ^{212}Po the error in the asymptotic Coulomb potential is a factor of ~ 1.01 , and we estimate that this will have a tiny effect on the results.

4. *α -particle wave function*: The simple form of the α -particle wave function used here is clearly a convenient approximation. One could consider more complicated forms obtained e.g. from the same nuclear structure model as used for the decaying nuclei. Although the present results are not very sensitive to the oscillator width taken for the α particle, the effect of having a more realistic wave function is difficult to estimate.
5. *Correlations*: As discussed in Sec. IIID a substantial increase in the formation amplitude can result from configuration mixing. For the case of ^{212}Po , shell-model calculations, e.g., [13, 23, 36] show better agreement for the absolute decay width than the present work. However as far as we know all these pioneering results have been based on schematic interactions often directly fitted to the nucleus being studied. A more systematic investigation of these effects using a globally valid interaction would thus be very interesting.

VI. CONCLUSIONS

We have performed a detailed microscopic calculation of α -decay widths. The mother and daughter nuclei were self-consistently described applying Skyrme's effective interaction, and the decay widths were calculated in the R -matrix formulation. Our results demonstrate that it is possible to obtain converged formation amplitudes employing a large harmonic oscillator basis. In contrast to standard observables such as masses, radii and excitation energies, these formation amplitudes probe the amount of cluster components present in the nuclear wave functions in the surface region. The results give a deeper understanding of the properties of the wave functions and suggest that a Skyrme-HFB treatment in combination with the R -matrix method is insufficient in order to predict absolute values of the α -decay lifetimes. Although one should note that there are several extensions to the formalism which can be envisioned and which seem to go in the right direction of shortening the too long lifetimes predicted. An improved description was also obtained by modifying the pairing interaction to increase the correlations in the nuclear surface. It is however difficult to determine the physical contents of such a prescription. In general we found that the pairing force is unable to give sufficient correlations to provide α particle formation amplitudes agreeing with data.

It is interesting to see that using a constant factor to renormalize the results leads to a close agreement with experimental data which is on par with the results from

purely semi-empirical formulas. This suggests that the missing effects, such as additional correlations needed to increase the probability of the α particle forming are in a first approximation proportional to the increase of the formation amplitudes obtained by including the pairing correlations. More work is needed in order to improve the model, for example by introducing more correlations, improvements in the decay formalism and/or treatments of continuum effects. The results presented here may then serve as a benchmark to evaluate the impact of such extended theories.

ACKNOWLEDGMENTS

B.G.C. and S.Å. thank the Swedish Research Council (VR) for financial support.

Appendix: Valence particle wave function

In this appendix we discuss the approximation used for the valence particles in Sec. II. The wave functions presented below are of shell model type, i.e., localized in the laboratory system, and thus contain contributions from the total center-of-mass motion of the nucleons. Such wave functions are written using a tilde, e.g., $\tilde{\Psi}(X)$. As there is no proton-neutron mixing, the HFB wave functions are products of proton and neutron HFB vacua. For each of the particle species we use the expansion given in Ref. [3] to express the mother nucleus as a function of the daughter. For the HFB case it becomes

$$|M; IM\rangle \approx \sum_{k < k'} X_{k,k'} c_k^\dagger c_{k'}^\dagger |D; jm\rangle, \quad (\text{A.1})$$

where proton and neutron indices have been omitted for clarity. The expansion coefficients are given by the two-particle transfer amplitudes,

$$X_{k,k'} = \langle M | c_k^\dagger c_{k'}^\dagger | D \rangle^*, \quad (\text{A.2})$$

where the c_k^\dagger operator creates a particle in state k , and k is a short-hand notation for the relevant spherical single-particle quantum numbers $nljm$. The two-particle transfer amplitudes are evaluated with the Onishi formula [41],

$$X_{kk'} = \langle M | c_k^\dagger c_{k'}^\dagger | D \rangle^* = \langle M | D \rangle^* \kappa_{k,k'}^{DM}, \quad (\text{A.3})$$

where the overlap $\langle M | D \rangle$ has an undetermined global phase, which we set to 1. This phase does not affect the calculated physical observables. The absolute value of the overlap is given by

$$|\langle M | D \rangle| = \left| \sqrt{\det \mathbf{U}} \right|. \quad (\text{A.4})$$

The pairing density, κ^{DM} , is given by

$$\kappa^{DM*} = -U_D^* (\mathbf{U}^T)^{-1} V_M^T, \quad (\text{A.5})$$

where \mathbf{U} is defined in terms of the U and V HFB matrices [41] of the mother and daughter states,

$$\mathbf{U} = U_D^\dagger U_M + V_D^\dagger V_M. \quad (\text{A.6})$$

Due to the spherical symmetry imposed on the HFB solutions the amplitudes simplify to,

$$X_{nljm,n'l'j'm'} = \delta_{j,j'} \delta_{l,l'} \delta_{m,-m'} (-1)^{j-m} X_{nn'}^{lj}, \quad (\text{A.7})$$

and the approximate neutron or proton part of the mother nucleus wave function can be written

$$|M; 00\rangle \approx \frac{1}{2} \sum_{lj} \sum_{nn'} \hat{j} X_{nn'}^{lj} \times \left[c_{nlj}^\dagger, c_{n'lj}^\dagger \right]_{00} |D; 00\rangle, \quad (\text{A.8})$$

where $I = M = 0$, and $\hat{j} = \sqrt{2j+1}$. The corresponding representation in coordinate space becomes

$$\tilde{\Psi}_{00}^M(X_{Z+2}) \approx \frac{1}{2} \sum_{lj} \sum_{nn'} \hat{j} X_{nn'}^{lj} \times \mathcal{A} \left\{ \left[\tilde{\phi}_{nlj}(\mathbf{r}_1), \tilde{\phi}_{n'lj}(\mathbf{r}_2) \right]_{00} \tilde{\Psi}_{00}^D(X_Z) \right\}, \quad (\text{A.9})$$

where X_Z and X_{Z+2} are coordinates for the daughter and mother nucleus, respectively. The approximate valence particle wave function is thus taken as

$$\tilde{\Phi}^{(v)}(\mathbf{r}_1, \mathbf{r}_2, \mathbf{r}_3, \mathbf{r}_4) = \tilde{\Phi}^{(v_\pi)}(\mathbf{r}_1, \mathbf{r}_2) \tilde{\Phi}^{(v_\nu)}(\mathbf{r}_3, \mathbf{r}_4), \quad (\text{A.10})$$

where

$$\tilde{\Phi}^{(v_q)}(\mathbf{r}_a, \mathbf{r}_b) = \frac{1}{2} \sum_{lj} \sum_{nn'} \hat{j} X_{nn'}^{q,lj} \times \mathcal{A} \left\{ \left[\tilde{\phi}_{nlj}(\mathbf{r}_a), \tilde{\phi}_{n'lj}(\mathbf{r}_b) \right]_{00} \right\}. \quad (\text{A.11})$$

- [1] Y. Oganessian, J. Phys G **34**, R165 (2007)
- [2] D. Rudolph, U. Forsberg, P. Golubev, L. G. Sarmiento, A. Yakushev, L.-L. Andersson, A. Di Nitto, C. E. Düllmann, J. M. Gates, K. E. Gregorich, C. J. Gross, F. P. Heßberger, R.-D. Herzberg, J. Khuyagbaatar, J. V. Kratz, K. Rykaczewski, M. Schädel, S. Åberg,

- D. Ackermann, M. Block, H. Brand, B. G. Carlsson, D. Cox, X. Derks, K. Eberhardt, J. Even, C. Fahlander, J. Gerl, E. Jäger, B. Kindler, J. Krier, I. Kojouharov, N. Kurz, B. Lommel, A. Mistry, C. Mokry, H. Nitsche, J. P. Omtvedt, P. Papadakis, I. Ragnarsson, J. Runke, H. Schaffner, B. Schausten, P. Thörle-Pospiech, T. Tor-

- res, T. Traut, N. Trautmann, A. Türler, A. Ward, D. E. Ward, and N. Wiehl, Phys. Rev. Lett. **111**, 112502 (2013)
- [3] R. Lovas, R. Liotta, A. Insolia, K. Varga, and D. Delion, Phys. Rep. **294**, 265 (1998)
- [4] D. S. Delion, *Theory of particle and cluster emission*, Lecture notes in physics No. 819 (Springer, 2010)
- [5] B. G. Carlsson, J. Toivanen, and U. von Barth, Phys. Rev. C **87**, 054303 (2013)
- [6] P. Descouvemont and D. Baye, Rep. Prog. Phys. **73**, 036301 (2010)
- [7] J. K. Poggenburg, H. J. Mang, and J. O. Rasmussen, Phys. Rev. **181**, 1697 (1969)
- [8] M. Bender, P.-H. Heenen, and P.-G. Reinhard, Rev. Mod. Phys. **75**, 121 (2003)
- [9] B. G. Carlsson, J. Dobaczewski, J. Toivanen, and P. Veselý, Comp. Phys. Commun. **181**, 1641 (2010)
- [10] J. Dobaczewski and P. Olbratowski, Comp. Phys. Commun. **158**, 158 (2004)
- [11] M. V. Stoitsov, J. Dobaczewski, W. Nazarewicz, and P. Ring, Comp. Phys. Commun. **167**, 43 (2005)
- [12] D. S. Delion, A. Insolia, and R. J. Liotta, Phys. Rev. C **54**, 292 (1996)
- [13] D. S. Delion and J. Suhonen, Phys. Rev. C **61**, 024304 (2000)
- [14] A. Insolia, R. J. Liotta, and E. Maglione, Europhys. Lett. **7**, 209 (1988)
- [15] M. Abramowitz and I. Stegun, *Handbook of Mathematical Functions*, Applied mathematics series (National Bureau of Standards, 1972)
- [16] G. Gamow, Z. Phys. **51**, 204 (1928)
- [17] J. Humblet and L. Rosenfeld, Nuclear Physics **26**, 529 (1961)
- [18] R. G. Thomas, Prog. of theo. phys. **12**, 253 (1954)
- [19] A. T. Kruppa and W. Nazarewicz, Phys. Rev. C **69**, 054311 (2004)
- [20] H.-D. Zeh, Z. Phys. **175**, 490 (1963)
- [21] H. J. Mang, Annu. Rev. Nucl. Sci. **14**, 1 (1964)
- [22] A. Bohm, M. Gadella, and G. B. Mainland, Am. J. Phys. **57**, 1103 (1989)
- [23] I. Tonozuka and A. Arima, Nucl. Phys. **A323**, 45 (1979)
- [24] J. Eichler and H.-J. Mang, Z. Phys. **183**, 321 (1965)
- [25] G. Kamuntavičius, R. Kalinauskas, B. Barret, S. Mickevičius, and D. Germanas, Nucl. Phys. **A695**, 191 (2001)
- [26] D. Vautherin and D. M. Brink, Phys. Rev. C **5**, 626 (1972)
- [27] K. Bennaceur and J. Dobaczewski, Comp. Phys. Commun. **168**, 96 (2005)
- [28] Y. Akaoli, Nuclear Data Sheets **84**, 1 (1998)
- [29] M. Samyn, S. Goriely, and J. Pearson, Nucl. Phys. **A725**, 69 (2003)
- [30] E. Chabanat, P. Bonche, P. Haensel, J. Meyer, and R. Schaeffer, Nucl. Phys. **A635**, 231; 643, 441(E) (1998)
- [31] P. Moller, J. Nix, W. Myers, and W. Swiatecki, At. Data Nucl. Data Tables **59**, 185 (1995)
- [32] C. Qi, F. R. Xu, R. J. Liotta, R. Wyss, M. Y. Zhang, C. Asawatangtrakuldee, and D. Hu, Phys. Rev. C **80**, 044326 (2009)
- [33] I. Muntian, Z. Patyk, and A. Sobiczewski, Phys. Atom. Nucl. **66**, 1015 (2003)
- [34] A. Sobiczewski, Private communication
- [35] D. S. Delion and A. Sandulescu, J. Phys G **28**, 617 (2002)
- [36] R. I. Betan and W. Nazarewicz, Phys. Rev. C **86**, 034338 (2012)
- [37] T. Fliessbach, Z. Phys. A **272**, 39 (1975)
- [38] T. Fliessbach and H. Mang, Nucl. Phys. **A263**, 75 (1976)
- [39] I. Tonozuka and A. Arima, Nucl. Phys. **A323**, 45 (1979)
- [40] G. F. Giuliani and G. Vignale, *Quantum theory of the electron liquid* (Cambridge university press, Cambridge, 2005)
- [41] P. Ring and P. Schuck, *The nuclear many body problem* (1st ed. Springer-Verlag, New York, 1980)